Progress In Electromagnetics Research, Vol. 135, 271–280, 2013

GRATING EFFECTS ON SIDELOBE SUPPRESSION IN MIM PLASMONIC FILTERS

Ramin Djabery[1, *], Saeid Nikmehr[1], and Shahram Hosseinzadeh[2]

[1]Faculty of Electrical and Computer Engineering, University of Tabriz, Tabriz, Iran

[2]Faculty of Engineering, Azarbaijan Shahid Madani University, 35 km Tabriz-Azarshahr Road, Iran

Abstract—In this paper a procedure for sidelobe suppression in the frequency response of a MIM (metal-insulator-metal) plasmonic filter is presented. Using the calculated effective refractive index for various values of the width of dielectric core and Bragg condition, the structural profile of primary filter is obtained. The frequency response for the transmission coefficient of the MIM plasmonic filter is derived by TRC-LOD-FDTD method. The variation in the frequency response of the filter due to changes in the structural parameters is studied. Finally, the usage of Gaussian, sinusoidal and linear types of gratings in suppressing the sidelobes and their effects on the stop-band bandwidth of the MIM plasmonic filter is investigated.

1. INTRODUCTION

In the past decade, plasmonic structures with ability to guide the light in a subwavelength scale have been received considerable attention [1]. The plasmonic structures, due to their unique characteristics, may find applications in integrated optics, bio detection, cloaking and so on [2].

Numerous researches have already been conducted on various aspects of this field. In [3], employing the full-wave electromagnetic theory, the electromagnetic scattering by a small cylindrical particle with radial anisotropy due to normally incident light of transverse magnetic (TM) polarization was investigated. An existence of a highly lossy interface mode (HLIM) in a designed plasmonic nanostructure for perfect absorption of the incident optical waves was reported in [4].

Received 28 October 2012, Accepted 18 December 2012, Scheduled 22 December 2012

* Corresponding author: Ramin Djabery (djabery@msn.com).

It was shown that, due to the HLIM lossy characteristic, surface plasmon polaritons would be significantly trapped at the TML (thin metallic layer) interface with absorption of nearly 100 percent. An idea of grating-based plasmon biosensor utilizing phase detection was presented in [5]. This idea was used in high resolution realization in finding a refractive index of a material located on the surface of a metal grating. In [6] the propagation properties of surface plasmon polaritons (SPP) and surface magnetoplasmon polaritons (SMP) modes in a semiconductor slit waveguide were analyzed by the effective dielectric constant approach. In [7] two metamaterials with sub-wavelength double-slots of single-and double-sides were proposed. The the electromagnetic resonance dependencies and local intensity enhancements on their structural parameters were also studied by finite-difference time-domain and finite element methods. The effect of geometry on the surface plasmon resonances was discussed in [8] and the character of the resonances with emphasis on a two-layer sphere were studied. In [9] the use of metamaterials to construct a surface plasmon sensor with application at microwave frequencies was discussed. A planar metallic nano structure design was the research subject of [10]. The proposed structure could support two distinct Fano resonances in its extinction cross-section spectrum under normally incident and linearly polarized electromagnetic field. The plane electromagnetic wave diffraction by an ideal metallic sphere (Mie's theory) was investigated in [11]. The proposed method involved representing the charge disturbances (polarization) by a displacement field in the positions of the mobile charges (electrons) and usage of the motion equation for the polarization along with electromagnetic potentials.

Despite the existence of different analysis techniques for plasmonic structures, the finite difference time domain (FDTD) method has received more attention [12]. In the FDTD method, a wide spectral response can be obtained using a single time analysis. Furthermore, the FDTD method requires using small spatial meshes for the analysis of plasmonic structures. However, when a traditional FDTD method is used in analysis, the computational time rises due to a small time steps that are determined by the Courant-Friedrich-Levy (CFL) condition. To eliminate the restriction of CFL condition in FDTD method, the locally one dimensional (LOD) scheme has been used in discretization of Maxwell's equations [13]. A three-dimensional FDTD method on graphics processing unit (GPU) for plasmonics applications is presented in [14].

Plasmonic structures are classified into two categories, insulator-metal-insulator (IMI) and metal-insulator-metal (MIM). Each one of

these structures has some advantages and disadvantages. Although, IMI structures have longer propagation length, they are not able to confine the light well into subwavelength geometries. MIM structures, on the other hand, have acceptable propagation length as well as higher confinement factor. By now some subwavelength optical devices such as waveguides, couplers and filters have been proposed [15].

In this paper, we have used the TRC-LOD-FDTD method of [13] to analyze a MIM plasmonic filter. Exciting the structure by a plane wave, we have obtained time response of the electric field at input and output planes of our primary filter. The transmission coefficient is calculated from the magnitude ratio of discrete Fourier transforms of electric fields at the output and input planes of filter. Finally, we have applied three different types of gratings to suppress its sidelobes.

2. DESIGN AND NUMERICAL RESULTS

2.1. Calculation of Effective Refractive Index

Figure 1 illustrates a schematic diagram of a MIM plasmonic waveguide which consists of a dielectric core region surrounded by two half infinite metal cladding. The TM polarization is assumed in analysis of this structure where only the fields components E_x, E_z and H_y are nonzero. From continuity of E_z and H_y along metal and dielectric interfaces, we obtain a dispersion relation as [16],

$$\tan(k_d a) = -\frac{k_m \varepsilon_d}{k_d \varepsilon_m} \tag{1}$$

where ε_d and k_d represent dielectric constant and transverse wave number of dielectric region and ε_m and k_m are dielectric function and transverse wave number of metal regions, respectively. The application

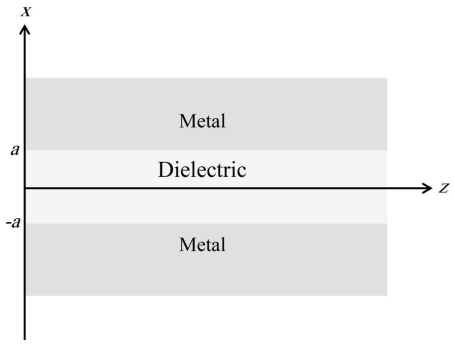

Figure 1. Geometry of a metal-insulator-metal structure.

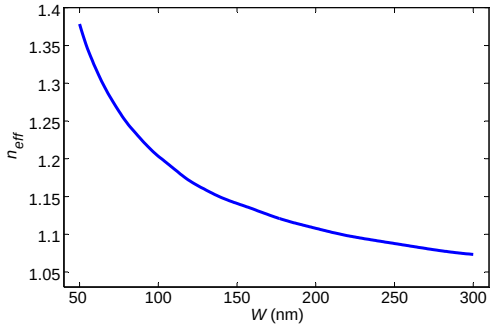

Figure 2. Effective refractive index as a function of dielectric core width for silver-air-silver structure.

of momentum conservation condition in each medium, yields the following relations between k_d, k_m and longitudinal wave number β.

$$\beta^2 - k_d^2 = \varepsilon_d k_0^2 \tag{2}$$

$$\beta^2 - k_m^2 = \varepsilon_m k_0^2 \tag{3}$$

where k_0 is the free space wave number. The parameters β, k_d and k_m are obtained by solving (1), (2) and (3). Then, the effective refractive index is calculated from,

$$n_{eff} = \frac{\mathrm{Re}[\beta]}{k_0} \tag{4}$$

Using (4), the values of n_{eff} are calculated for various values of dielectric core width ($W = 2a$) of the silver-air-silver structure and plotted in Figure 2. As it is obvious from this figure, n_{eff} decreases when dielectric core width is increased. These values of effective refractive index will be used in our later MIM plasmonic filter design.

2.2. Filter Design

Figure 3 illustrates the silver-air-silver plasmonic filter with periodic changes in dielectric core width.

In the procedure of designing a MIM plasmonic filter, the parameters L_1, L_2, n_{eff_1} and n_{eff_2} should be determine. The following relation has been obtained using the Bragg condition of [16].

$$2(n_{eff_1} L_1 + n_{eff_2} L_2) = (2m + 1)\lambda \tag{5}$$

According to the usual operating frequency in optical communication systems, the wavelength, λ, is assumed to be 1.55 µm. Since, the objective is designing a filter for symmetric modes, the width of the

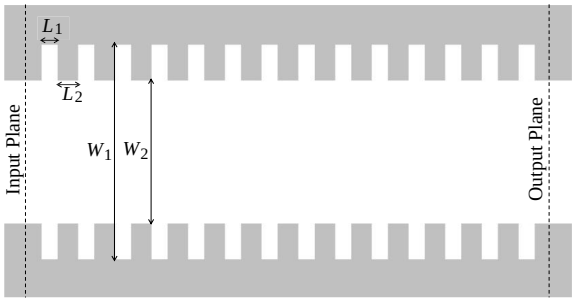

Figure 3. MIM plasmonic filter with periodic changes in the width of dielectric core.

dielectric core, according to [17], is considered to be more than 100 nm. Therefore, the values of W_1 and W_2 are chosen to be 100 nm and 150 nm, respectively. Thus, for these choices of W_1 and W_2, the values of respective effective refractive indexes may be obtained from Figure 2 as: $n_{eff_1} = 1.139$ and $n_{eff_2} = 1.2$. Using the lower order Bragg condition ($m = 0$) and the acquired values of $n_{eff_{1(2)}}$ in (5), we obtain the period lengths of $L_1 = 292$ nm, $L_2 = 368$ nm. Based on numerical experiments, the number of grating period is chosen to be equal to 14. After determining the structural parameters, we can proceed to the time domain analysis of the filter.

The dielectric function of silver, using Drude model, may be expressed as,

$$\varepsilon_r(\omega) = \varepsilon_\infty - \frac{\omega_p^2}{\omega^2 - j\gamma\omega} \tag{6}$$

where ω_p is the electron plasma frequency, ε_∞ the dielectric constant at infinite frequency, and γ the collision frequency. The dispersion of silver region is taken into account by Drude model with $\varepsilon_\infty = 3.7$, $\omega_p = 9.1$ ev and $\gamma = 0.018$ ev [18]. The sampling widths of $\Delta x = 5$ nm, $\Delta z = 4$ nm are considered. The upper limits of CFL condition and CFL number (CFLN) are 0.0103 fs and $\frac{\Delta t}{\Delta t_{CFL}}$, respectively. The total-field, scattered-field formulation method of [12] is used to implement the plane wave excitation with the Gaussian Pulse width of 100–300 THz.

Time variations of E_x in the input and output planes are calculated with TRC-LOD-FDTD method for CFLN = 10, and depicted in the Figure 4.

The transmission coefficient calculated from the magnitude ratio of discrete Fourier transforms of the electric fields at the output and input planes of filter. The transmission coefficient for primary MIM plasmonic filter is illustrated in Figure 5. In order to validate our

analysis, the simulation result of [19] is added to Figure 5. It is obvious that there is a good conformity between results.

Our primary MIM plasmonic filter has been designed for central wavelength of $\lambda = 1.55\,\mu m$. However, design for other frequencies could easily be carried out by varying the structural parameters. For specific value of central wavelength, changing either one of L_1, L_2, n_{eff_1} and n_{eff_2} in (5) would serve for this purpose. Note that, changing n_{eff_1} and n_{eff_2} requires redetermining the corresponding values of W_1 and W_2

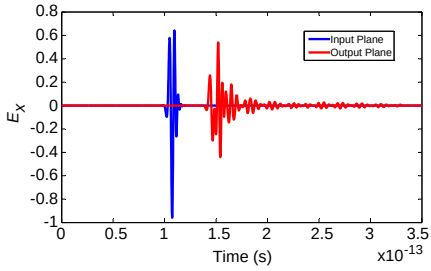

Figure 4. Time variation of E_x at the input and output planes.

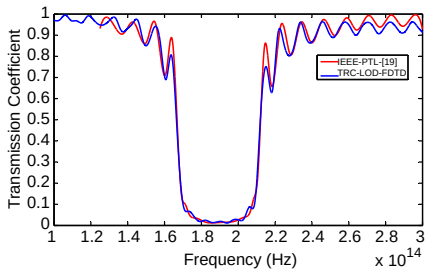

Figure 5. Transmission coefficient of primary MIM plasmonic filter.

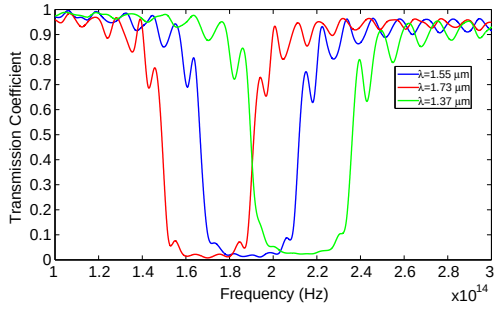

Figure 6. Transmission coefficients for $\lambda = 1.37\,\mu m$, $\lambda = 1.55\,\mu m$ and $\lambda = 1.73\,\mu m$.

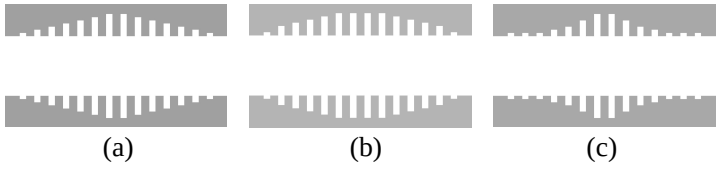

Figure 7. Geometry of MIM plasmonic filter with (a) linear grating, (b) sinusoid grating, and (c) Gaussian grating.

from Figure 2. For example, in order to move the central wavelength to $\lambda = 1.37\,\mu m$ and $\lambda = 1.73\,\mu m$, the values of $L_1 = 212\,nm$ and $L_1 = 372\,nm$ may be calculated from (5), respectively, while other three parameters are kept at their previous values. The transmission coefficients for these three values of central wavelengths are depicted in Figure 6. As it can be observed from this figure, the frequency response is shifted according to the respected choice of central wavelength, while

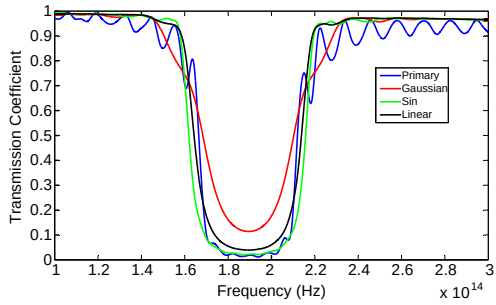

Figure 8. Transmission Coefficient of primary and grated MIM plasmonic filter.

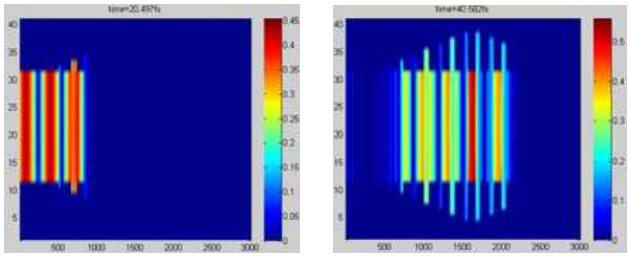

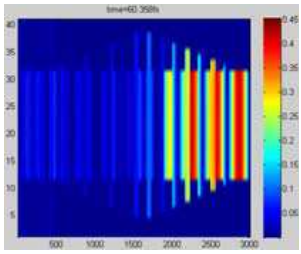

Figure 9. Snapshots of electric field for $f = 100\,THz$ (outside the bandgap) at (a) $t = 20.497\,fs$, (b) $t = 40.582\,fs$, and (c) $t = 60.358\,fs$.

its overall shape is virtually preserved.

It can be seen from Figures 5 and 6 that there are many sidelobes in the frequency response of the filter. In order to improve the performance of this filter, we have applied three different gratings of Figure 7 to its structure. The transmission coefficients of these modified and original MIM palsmonic filters are depicted in the Figure 8. It is obvious that sidelobes are suppressed with employing any one of these gratings. For Gaussian type grating, the bandwidth and the attenuation in stop band region are decreased while in the case of linear grating this decrement is negligible. For sinusoidal grating the bandwidth is slightly increased while the stop band attenuation is not affected. Therefore, it can be concluded that the linear grating has the best frequency response.

To have a better perception of the filtering characteristics, snapshots of the transmitted electromagnetic patterns at several time steps are included for the case of linear grating. In Figures 9 and 10 the electric field distribution inside the MIM plasmonic filter are plotted at 193 and 100 THz. It is clear that, the wave with the frequency of 100 THz which is outside the bandgap, is transmitted and the wave with the frequency of 193 THz which is inside, is not transmitted.

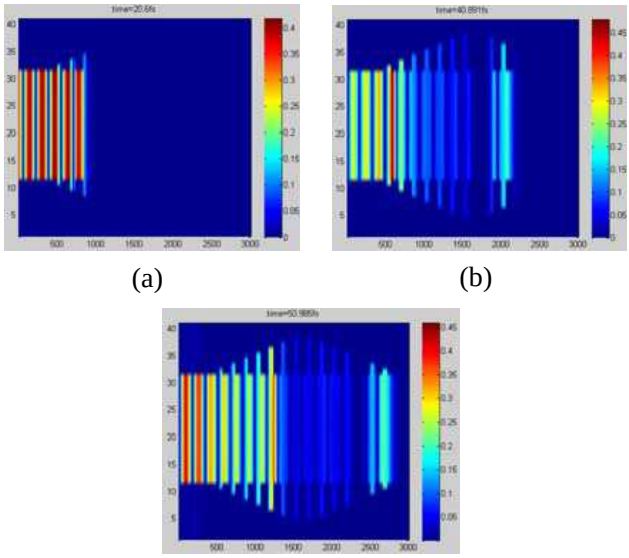

(a) (b)

(c)

Figure 10. Snapshots of electric field for $f = 193$ THz (inside the bandgap) at (a) $t = 20.6$ fs, (b) $t = 40.891$ fs, and (c) $t = 50.985$ fs.

3. CONCLUSION

We have presented a procedure for sidelobe suppression of a MIM plasmonic filter. The effective refractive index was calculated for various values of the dielectric core width of the MIM structure. Using the calculated values of effective refractive index and Bragg condition, the structural profile of primary filter was obtained. Next, the TRC-LOD-FDTD method of analysis was applied to the MIM plasmonic filter and the transmission coefficient was derived. The effects of varying the structural parameters on the frequency response of the filter was studied. Finally, we have applied Gaussian, sinusoidal and linear types of gratings to the structure of the primary MIM plasmonic filter. The effects of these gratings on suppression of the sidelobes were investigated.

REFERENCES

1. Barnes, W. L., A. Dereux, and T. W. Ebbesen, "Surface plasmon subwavelength optics," *Nature*, Vol. 424, 824–830, 2003.
2. Maier, S. A., *Plasmonics Fundamental and Applications*, Springer-Verlag, New York, 2007.
3. Jin, Y. W., D. L. Gao, and L. Gao, "Plasmonic resonant light scattering by a cylinder with radial anisotropy," *Progress In Electromagnetics Research*, Vol. 106, 335–347, 2010.
4. Gong, Y., "Frequency-selective nanostructured plasmonic absorber by highly lossy interface mode," *Progress In Electromagnetics Research*, Vol. 124, 511–525, 2012.
5. Luo, Z., "A grating-based plasmon biosensor with high resolution," *Progress In Electromagnetics Research*, Vol. 118, 527–539, 2011.
6. Kong, F. M. and K. Li, "Analysis of the surface magnetoplasmon modes in the semiconductor slit waveguide at terahertz frequencies," *Progress In Electromagnetics Research*, Vol. 82, 257–270, 2008.
7. Han, L., "Calculation and optimization of electro-magnetic resonances and local intensity enhancements for plasmon metamaterials with sub-wavelength double-slots," *Progress In Electromagnetics Research*, Vol. 113, 161–177, 2011.
8. Sihvola, A., "Character of surface plasmons in layered spherical structures," *Progress In Electromagnetics Research*, Vol. 62, 317–331, 2006.
9. Ishimaru, A., "Generalized surface plasmon resonance sensors

using metamaterials and negative index materials," *Progress In Electromagnetics Research*, Vol. 51, 139–152, 2005.

10. Amin, M., "Investigation of Fano resonance induced by higher order plasmon modes on a circular nano-disk with an elongated cavity," *Progress In Electromagnetics Research*, Vol. 130, 187–206, 2012.
11. Apostol, M., "Plasmons and diffraction of an electro-magnetic plane wave by a metallic sphere," *Progress In Electromagnetics Research*, Vol. 98, 97–118, 2009.
12. Taflove, A. and S. C. Hagness, *Computational Electrodynamics: The Finite-difference Time-domain Method*, 3rd Edition, Artech House, Norwood, MA, 2005.
13. Shibayama, J., "Frequency-dependent LOD-FDTD method and its application to the analyses of plasmonic waveguide devices," *IEEE J. Quantum Electronics*, Vol. 46, No. 1, 40–49, 2010.
14. Lee, K. H., "Implementation of the FDTD method based on Lorentz-Drude dispersive model on GPU for plasmonics applications," *Progress In Electromagnetics Research*, Vol. 116, 441–456, 2011.
15. Chen, P., "Plasmonic filters and optical directional couplers based on wide metal-isulator-metal structure," *Optics Express*, Vol. 19, No. 8, 2011.
16. Park, J., "High order plasmonic Bragg reflection in the metal-isulator-metal waveguide Bragg grating," *Optics Express*, Vol. 16, No. 1, 2008.
17. Dionne, J., "Plasmon slot waveguides towards chip-scale propagation with subwavelength-scale localization," *Physical Review B*, Vol. 73, No. 3, 2008.
18. Djabery, R., S. Nikmehr, and S. Hosseinzadeh, "Simple algorithm for calculation of trapezoidal recursive convolution-locally 1-D finite-difference time-domain equations at metal-dielectric interface," *Photonics Technology Letters*, Vol. 24, No. 20, 1827–1829, 2012.
19. Zhanghua, H., "Surface plasmon bragg gratings formed in metal-insulator-metal waveguides," *Photonics Technology Letters*, Vol. 19, No. 2, 2007.